Asian Journal of Pharmaceutical Sciences 15 (2020) 518–528

Available online at www.sciencedirect.com

ScienceDirect

journal homepage: www.elsevier.com/locate/AJPS

Original Research Paper

Enhancement of oral bioavailability and anti-Parkinsonian efficacy of resveratrol through a nanocrystal formulation

Sha Xiong[a,1], *Wei Liu*[a,1], *Yile Zhou*[a], *Yousheng Mo*[a], *Yao Liu*[a], *Xiaojia Chen*[b], *Huafeng Pan*[a], *Dongsheng Yuan*[a,*], *Qi Wang*[a,*], *Tongkai Chen*[a,*]

[a] *Institute of Clinical Pharmacology, Guangzhou University of Chinese Medicine, Guangzhou 510405, China*
[b] *Institute of Chinese Medical Sciences, University of Macau, Macau, China*

ARTICLE INFO

Article history:
Received 5 December 2018
Revised 7 April 2019
Accepted 17 April 2019
Available online 24 May 2019

Keywords:
Nanocrystals
Resveratrol
Oral absorption
Brain permeability
Anti-Parkinsonian efficacy

ABSTRACT

Resveratrol (RES), a non-flavonoid polyphenol extracted from a wide variety of plants, exhibits neuroprotective activities against Parkinson's disease (PD). However, undesirable water solubility of RES reduces its oral bioavailability and demonstrates low efficacy in blood and brain, thus limiting its application. In present study, a nanocrystal formulation of RES (RES-NCs) was developed to enhance its oral bioavailability and delivery into brain for PD treatment. RES-NCs were fabricated with hydroxypropyl methylcellulose (HPMC) stabilizer via antisolvent precipitation approach. The obtained RES-NCs displayed the particle size of 222.54 ± 1.66 nm, the PDI of 0.125 ± 0.035, the zeta potential of −9.41 ± 0.37 mV, and a rapid *in vitro* dissolution rate. Molecular dynamics simulation of RES and HPMC revealed an interaction energy of −68.09 kJ/mol and a binding energy of −30.98 ± 0.388 kJ/mol, indicating that the spontaneous binding between the two molecules is through van der Waals forces. RES-NCs conferred enhanced cellular uptake as well as improved permeability relative to pure RES. In addition, RES-NCs were able to protect neurons against cytotoxicity induced by MPP^+. Meanwhile, RES-NCs exerted no significant toxic effects on zebrafish embryos and larvae, and did not influence their survival and hatching rates. When orally administered to rats, RES-NCs exhibited more favorable pharmacokinetics than pure RES, with higher plasma and brain concentrations. More importantly, MPTP-induced PD mice showed notable improvements in behavior, attenuated dopamine deficiency, and elevated levels of dopamine and its metabolites after the treatment with RES-NCs. Furthermore, immunoblot analysis revealed that the neuroprotective role of RES-NCs may be at least partially mediated

* Corresponding authors. Institute of Clinical Pharmacology, Guangzhou University of Chinese Medicine, 12 Jichang Road, Guangzhou 510405, China.
E-mail addresses: yds@gzucm.edu.cn (D.S. Yuan), wangqi@gzucm.edu.cn (Q. Wang), chentongkai@gzucm.edu.cn (T. Chen).
[1] These authors contributed equally to this work.
Peer review under responsibility of Shenyang Pharmaceutical University.

https://doi.org/10.1016/j.ajps.2019.04.003

by Akt/Gsk3β signaling pathway. Taken altogether, RES-NCs can serve as a potential treatment modality for PD, offering means of improving RES oral bioavailability and brain accumulation.

1. Introduction

Parkinson's disease (PD) is an extremely common neurodegenerative disease, which affects 2% of the elderly population (≥ 65 years old) [1]. This disease is accompanied by striatal dopamine (DA) deficiency and neuronal loss in the substantia nigra [2]. PD is placing substantial medical and social burdens on patients and their caregivers. Current approaches for treating PD are aimed at slowing its progression, improving motor function, and decreasing the motor symptoms of the patients [3]. Despite these efforts, undesirable oral bioavailability and limited brain penetration of PD drugs may prohibit them from exerting their therapeutic effects [4,5]. Thus, in order to address the unmet clinical needs, the major active constituents of herbal drugs have been investigated for the potential treatment of PD [6,7].

Resveratrol (RES), a non-flavonoid polyphenol extracted from a wide variety of plants, may exert neuroprotective effects on the treatment of PD [8]. Many studies have determined that RES can protect against neurotoxic destruction of dopaminergic neurons in response to 6-hydroxydopamine or 1-methyl-4-phenyl-1,2,3,6-tetrahydropyridine (MPTP), owing to its ability to disrupt the degeneration of tyrosine hydroxylase positive (TH^+) dopaminergic neurons [9,10]. This activity is thought to be mediated via an Akt/Gsk-3β signaling pathway, ultimately leading to a reduction in rates of cell death in PD model systems [11]. RES is a poorly water-soluble natural product with high membrane permeability [12], and has been considered as a Class II compound based on the Biopharmaceutical Classification System (BCS). In recent years, a wide variety of strategies have been implemented in an effort to increase RES bioavailability, including sericin nanoparticles [13], solid lipid nanoparticles [14], colloidal mesoporous silica nanoparticles [15] and galactosylated PLGA nanoparticles [16]. However, the use of these formulations has been limited in clinical practice, due to their necessity for numerous additives and a dearth of relevant pharmacokinetic data regarding their brain penetration. As such, there is a clear need for an alternate formulation which may improve RES oral bioavailability and brain uptake.

Nanocrystals are drug crystals with sizes in the scale of 1–1000 nm, which can ameliorate the dissolution rates and absorption of BCS Class II drugs by increasing specific surface and improving saturated solubility [17]. Typically, drug nanocrystals can be obtained from different particle size reduction techniques (i.e. top-down and bottom-up), depending on the drug properties and production parameters [18]. The top-down approach depends upon reducing particle size through media milling, micro-fluidization, high-pressure homogenization, etc. However, the disadvantages associated with this approach are the existence of high energy and the formation of large crystals following rapid precipitation [19]. Besides, through bottom-up approach, drug nanocrystals are prepared by solvent/antisolvent precipitation method in the presence of a stabilizer, leading to smaller size and more homogenous particles [20]. Therefore, in this study, antisolvent precipitation approach was applied during the preparation of RES nanocrystals (RES-NCs).

Thus far, a variety of nanocrystal drug products have entered the market, such as Invega Sustenna®, Theodur®, Naprelan®, and Megace ES® [21]. However, the interaction between drug and stabilizer is not completely understood. Therefore, in the present study, we utilized molecular dynamics simulation to better understand how RES binds to stabilizer. We also assessed the toxic effects of RES-NCs *in vitro* using Madin-Darby canine kidney (MDCK) and SH-SY5Y cell lines, and *in vivo* using zebrafish model. Furthermore, RES-NCs were subjected to rat pharmacokinetic investigation, and their anti-Parkinsonian efficacy was evaluated in MPTP-induced PD mouse model.

2. Materials and methods

2.1. Materials

RES, 3-(4, 5-dimethylthiazol-2-yl)−2, 5-diphenyltetrazolium bromide (MTT), rabbit polyclonal anti-TH antibody, 1-methyl-4-phenyl-1,2,3,6-tetrahydropyridine (MPTP), 1-methyl-4-phenylpyridinium ion (MPP^+) and Selegiline were all obtained from Sigma-Aldrich (St. Louis, USA). Hydroxypropyl methylcellulose (HPMC) with a viscosity of 50 cps was kindly supplied by Colorcon Co., Ltd. (Shanghai, China). MDCK and SH-SY5Y cells were provided by Guangzhou Jenniobio Biotechnology Co., Ltd. (Guangzhou, China). Anti-rabbit IgG, anti-Akt, anti-phospho-Akt (Ser473), anti-Gsk3β and antiphospho-Gsk3β (Ser9) antibodies were purchased from Cell Signaling Technology (Danvers, USA).

2.2. Preparation and characterization of RES-NCs

As aforementioned, we used antisolvent precipitation technique and stabilizer-based approach to prepare RES-NCs [22]. Briefly, we injected 500 ul of RES (10 mg/ml in acetone) to 10 ml of polyvinylpyrrolidone K90 (PVP K90, 1 mg/ml in H_2O), and this mixture was stirred at room temperature at 800 rpm. To evaluate the effects of each parameter (including stabilizers types and concentrations, the drug concentrations and the volume ratios of the antisolvent to the solvent) on

short-term stability, single factor design was then used to establish the most ideal nanocrystal formulation. After that, dynamic light scattering (DLS) was performed to measure the particle size, polydispersity index (PDI) and zeta potential of the optimized RES-NCs. Meanwhile, the thermal and crystalline properties were also determined. For detailed methods regarding the characterization of RES-NCs, see Supporting Information, section S1.

2.3. *In vitro dissolution study*

We assessed how RES-NCs dissolve based on a dialysis approach [23]. One millilitre of RES, RES-NCs, or a combination of RES and HPMC (RES-PM) was added to a 3.5 kDa MWCO dialysis bag. The bags were then placed into 50 ml media containing both 0.1 mol/l HCl and 0.1% sodium dodecyl sulfate (SDS) to simulate a gastric environment. After shaking at 100 r/min and 37 °C, one millilitre of dialysis medium was removed at 1, 5, 10, 15, 20, 25, 30, 45 and 60 min, and immediately replaced with fresh medium. Finally, the content of RES was measured by Agilent 1100 series high performance liquid chromatography (HPLC) system with an Eclipse XDB C_{18} column (4.6 mm × 250 mm, 5 µm). The mobile phase was mixture of water and methanol (30:70, v:v) containing 0.5% acetic acid. Samples (20 µl) were injected to the column and underwent elution for 8 min at 1.0 ml/min. Ultraviolet detection was set at 306 nm.

2.4. *Molecular dynamics simulation*

We used ChemDraw to construct the molecular structures of RES and HPMC based on MMFF94x Force Field parameters. The Gaussian09 package was used to optimize the atoms of these molecules at the HF/6–31G* level. Subsequently, the partial atomic charges of RES and HPMC were calculated according to the restrained electrostatic potential (RESP) charge. Afterwards, the complexes were neutralized using sodium/chlorine counter ions, and the molecules then underwent solvation with TIP3P water molecules. AMBER16 was used in order to perform a molecular dynamics simulation. In addition, AMBER GAFF and AMBER14SB along with SHAKE algorithm were used to constrain covalent bonds containing hydrogen at a 2 fs time step. Long range electrostatic interactions were assessed via a Particle Mesh Ewald approach, while energy minimization was conducted in two steps, as in previous report [24]. Over a 40 ns period, we used a Molecular Mechanics Poisson-Boltzmann Surface Area (MM-PBSA) approach to explore HPMC/RES binding energies.

2.5. *Assessment of RES-NCs cellular uptake and transport*

We used an MTT assay to assess MDCK cell viability after RES or RES-NCs treatment (See Supporting Information, section S2). We also assessed cellular uptake of RES-NCs by these MDCK cells and measured the apparent permeability coefficient (P_{app}) (See Supporting Information, section S2).

2.6. *Assessment of RES-NCs protection against MPP^+-mediated cell death*

We seeded SH-SY5Y cells in 96-well plates (5000 cells/cm^2) for 24 h, and then pretreated cells using 1–20 µM of RES-NCs or control for 2 h, after which cells were incubated with 2 mM MPP^+ for 24 h. Finally, we measured cell viability via MTT assay as described above.

2.7. *Evaluation of in vivo RES-NCs toxicity*

A range of RES-NCs concentrations (0–150 µg/ml) were chosen to treat zebrafish embryos at 6 h post fertilization (hpf; $n = 20$ per condition) in 24-well plates. These concentrations were selected in accordance with the OECD Guidelines of the Testing of Chemicals and to meet the statistical requirements. Every 24 h, we replaced the media in these wells, and embryo morphology was monitored via microscopy (DMi8, Leica, Germany). At 72 hpf, we calculated survival and hatching rates. For more information regarding zebrafish experiments, see Supporting Information, section S3.

2.8. *Pharmacokinetic analysis of RES-NCs in rats*

RES-NCs pharmacokinetics were conducted using Sprague-Dawley (SD) rats (6–8 weeks, males). All experiments were approved by University Animal Ethics Committee. We housed rats in a standard 12:12-h light:dark cycle at 25 ± 2 °C, in the environment with 55% ± 5% relative humidity and free food/water access. Rats were dosed orally with either RES-NCs (4 mg/kg RES) or an equivalent RES dose in 1.8 mg/ml HPMC (controls). We collected serum samples from these rats via 300 µl of tail vein blood ($n = 6$ per time point) at times from 0–24 h. Samples were spun at 5000 rpm for 5 min, and supernatants were taken for analysis. We also collected brain samples from rats at 0, 0.5, 1, 2, 4, 8, 12 and 24 h. At these time points, we anesthetized the animals, perfused them with physiological saline, removed the entire brain ($n = 3$ per time point), weighed the tissue, and then homogenized it in cold saline using a tissue homogenizer. For more detail regarding these protocols, refer to Supporting Information, section S4. RES concentrations in these samples were then assessed via HPLC as described above.

We used the DAS (Drug and Statistics) v2.0 to perform a non-compartmental analysis which allowed us to calculate key parameters including: peak RES-NCs concentrations in the brain/plasma (C_{max}), time to peak RES-NCs concentrations (T_{max}), RES-NCs half-life ($T_{1/2}$), AUC for a concentration-time curve of RES-NCs ($AUC_{0\text{-}t}$), and mean residence time ($MRT_{0\text{-}t}$). We also calculated RES-NCs relative bioavailability (F) relative to RES based on the following Eq. 1:

$$F = \frac{AUC_{RES-NCs}}{AUC_{control\ group}} \times 100\% \quad (1)$$

2.9. Assessment of RES-NCs neuroprotective effects in a PD mouse model

8-week-old male C57BL/6 mice (22–25 g) were housed under the same standard conditions as described for rats above. All mice were separated into 5 groups: a RES-NCs group, a RES group, a Selegiline group, an MPTP group, and a control group. PD was induced in these mice via intraperitoneally injecting 18 mg/kg MPTP (in 0.9% saline) in 4 total doses, each spaced 2 h apart. Mice were administered RES in 1.8 mg/ml HPMC or RES-NCs (with both groups receiving a dose of RES of 5 mg/kg) via gavage over a 14-d period. Treatments were once daily prior to MPTP treatment, and twice daily thereafter for 7 d in each condition. Control animals received 0.9% saline, while selegiline mice were dosed i.p. using a preparation of 10 mg/kg seligiline in 0.9% saline (q.d. over a 7-d period). The neuroprotection of RES-NCs in these mice were assessed based on PD behavioral testing, and total TH^+ neuron numbers were calculated, and while levels of DA and its metabolites were quantified. For details regarding these measurements, see Supporting Information, section S5.

2.10. Assessment of the Akt/Gsk3β signaling pathway in PD model mice

We used radio-immunoprecipitation assay (RIPA) buffer to extract total protein from murine samples in the presence of protease/phosphatase, and protein levels were quantified via BCA Protein Assay Kit. Equivalent quantities (20 μg) of samples were then electrophoretically separated via 10% SDS-PAGE (SDS-polyacrylamide gel electrophoresis), followed by transfer onto polyvinylidene fluoride (PVDF) membranes which were blocked using 5% BSA. Membranes were then probed overnight using 1:1000 dilutions of antibodies against Akt, p-Akt (Ser473), Gsk3β, and p-Gsk3β (Ser9) at 4 °C. Blots were washed thrice in TBST (Tris-buffered saline with 0.05% Tween-20), and then probed for 2 h with appropriate secondary HRP-conjugated antibodies at room temperature. Enhanced chemiluminescence was used for protein band visualization. All data were plotted as the percentage of normalized phosphorylation level (phospho-Akt at Ser473 or phospho-Gsk3β Ser9) over normalized total protein concentration (Akt or Gsk3β).

2.11. Statistical analysis

Results were compared via one- or two-way analyses of variance (ANOVA). All data were presented as means ± SD. $P < 0.05$ was the significance threshold.

3. Results and discussion

3.1. Preparation and characterization of RES-NCs

The short-term stability of RES-NCs formulations were evaluated by adding five different stabilizers, such as HPMC, PVP K90, D-α-tocopheryl polyethylene glycol 1000 succinate (TPGS), Poloxamer 407, and Tween 80. It was found that HPMC-stabilized RES-NCs demonstrated the lowest precipitation (Fig. S1A). We then further assessed how HPMC concentrations influenced the short-term stability of RES-NCs, determining that 1.8 mg/ml HPMC was able to result in minimal precipitation over a 24 h period (Fig. S1B). In addition, we found that increasing the RES concentration from 5 to 20 mg/ml had no influence on short-term stability (Fig. S1C), leading us to select 20 mg/ml RES as an optimal drug concentration. We also assessed how short-term stability of these nanocrystals was altered by different antisolvent to solvent ratios (from 10:1 to 50:1), revealing that at a 40:1 ratio these RES-NCs were stable without detectable precipitation over a 24 h period, leading us to select this ratio for use in the remainder of the study (Fig. S1D). As a whole, the optimized RES-NCs were established through rapid injection of 0.25 ml acetone (organic solvent) containing 20 mg/ml RES into 1.8 mg/ml HPMC in 10 ml H_2O (antisolvent) at a stirring speed of 800 r/min and room temperature.

For the optimized RES-NCs, the particle size was 222.54 ± 1.66 nm, the PDI was 0.125 ± 0.035, the zeta potential was −9.41 ± 0.37 mV, and the loading capacity was 21.74% (Fig. 1A and Fig. S2). These RES-NCs were irregular in shape, as demonstrated in TEM images (Supporting Information, Fig. S3). TEM sizing estimates were smaller than those obtained via DLS (205 nm *vs.* 222 nm), which may be due to the fact that TEM images detect dry crystals whereas DLS is dependent on the hydrodynamic size of particles in solution. Meanwhile, the DSC (differential scanning calorimetry) profiles of RES-NCs, RES and RES-PM revealed a single endothermic peak at 230 °C melting point (Fig. 1B), indicating that RES was obtained in crystalline form. The PXRD (powder X-ray diffraction) patterns of RES-NCs, RES alone and RES-PM demonstrated the relatively similar crystalline diffraction peaks of 6.64°, 13.28°, 16.38° and 19.24°, respectively (Fig. 1C). Collectively, the results of DSC and PXRD strongly suggest that the precipitation process does not influence the RES crystalline state within these RES-NCs. Besides, the *in vitro* dissolution of RES-NCs was apparently different from that of RES or RES-PM. Notably, RES-NCs exhibited a fast dissolution rate within 25 min, in which 93.1% of RES were released from RES-NCs compared to less than 25% of RES released from RES-PM or RES itself after 1 h (Fig. 1D). Considering the rapid dissolution rate of RES-NCs, simulated gastric media was selected as the dissolution medium in the present study. This rapid dissolution rate was likely attributable to their reduced particle size and increased surface area of RES-NCs, consistent with the Noyes-Whitney equation [22].

3.2. Molecular dynamics simulation

To assess the binding and interaction between RES and HPMC, molecular dynamics simulation was performed on these two molecules in the presence of excess H_2O. Fig. 2A showed the interaction between RES and HPMC at 0, 13, 26, and 37 ns. The distances in the center of mass between RES and HPMC revealed an interaction between the two molecules in the beginning of the initial conformation (Fig. 2B). Following the interaction, the stability of RES-HPMC complex remained high until ~26 ns. From ~26.5 – ~29.5 ns, a momentary break was found in the interaction between the two molecules, followed by reestablishing their interaction through the end of the simulation period.

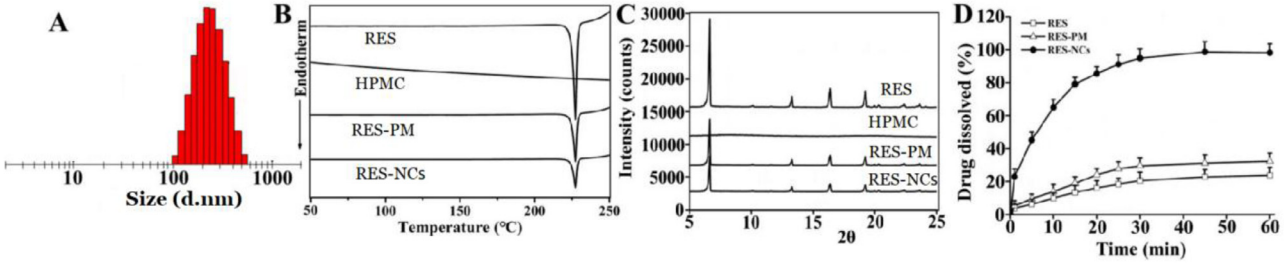

Fig. 1 – Characterization of RES-NCs. (A) Distribution of particle size; (B) DSC profiles; (C) PXRD patterns; (D) Dissolution profiles. The data are presented as means ± SD ($n = 3$).

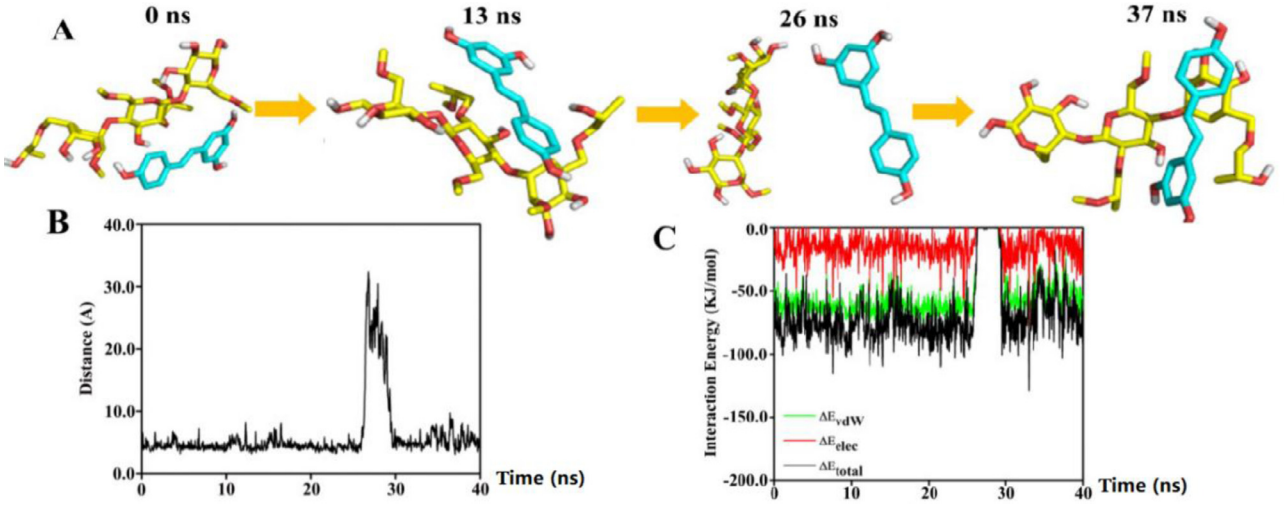

Fig. 2 – Molecular dynamics simulation of RES and HPMC with excess H_2O. (A) The structures of RES and HPMC at 0, 13, 26, and 37 ns. Both molecules are illustrated in a stick model. HPMC is represented by yellow, while RES is cyan. (B) Distances between centers of mass of RES and HPMC over time. (C) Changes in RES/HPMC interaction energies over time.

We also assessed variations over time between these molecules with respect to electrostatic interaction energies and van der Waals (vdW) forces (Fig. 2C). The average interaction energy between RES and HPMC was ~−68.09 kJ/mol from 0 to 40 ns. All the interaction energy components demonstrated that the spontaneous binding between RES and HPMC was largely governed by vdW interaction. vdW and electrostatic interactions contributions to binding free energy (ΔG_{total}) were given as ΔE_{vdW} and ΔE_{elec}, while polar and nonpolar solvation energy contributions to ΔG_{total} were given as ΔG_{polar} and $\Delta G_{nonpolar}$. The binding between RES-HPMC was largely governed by hydrophobic interaction, with ΔE_{vdW} being the most favorable contributor. As shown in Table 1, the value of ΔG_{polar} (44.297 ± 0.519 kJ/mol) indicated an unfavorable contribution to the binding, whereas $\Delta G_{nonpolar}$ (−7.189 ± 0.071 kJ/mol) contributed favorably to the binding. The average value of ΔG_{total} was found to be −30.98 ± 0.388 kJ/mol, indicating an overall favorable binding energy.

Table 1 – RES-HPMC binding energies.

Contribution	Energy (kJ/mol)
ΔE_{vdW}	−53.614 ± 0.568
ΔE_{elec}	−14.473 ± 0.341
ΔG_{polar}	44.297 ± 0.519
$\Delta G_{nonpolar}$	−7.189 ± 0.071
ΔG_{total}	−30.98 ± 0.388

3.3. *Cellular uptake and transport study*

The results of MTT assay revealed no significant *in vitro* cytotoxic effect of RES-NCs on MDCK cells at different treatment concentrations (1–200 μM) (Supporting Information, Fig. S4). The cellular uptake of RES was significantly increased in RES-NCs group (2.26 ± 0.04 μg/mg) compared to RES group (1.28 ± 0.05 μg/mg) and RES-PM group (1.47 ± 0.09 μg/mg). Moreover, the value of P_{app} was higher in RES-NCs ($3.79 \pm 0.19 \times 10^{-5}$ cm/s) group compared to RES group ($1.26 \pm 0.14 \times 10^{-5}$ cm/s) and RES-PM group ($1.40 \pm 0.17 \times 10^{-5}$ cm/s), suggesting that these RES-NCs are better able to transport RES across MDCK cell monolayers. However, there was no significant difference in the transport of RES between RES-NCs group ($3.79 \pm 0.19 \times 10^{-5}$ cm/s) and RES dissolved in dimethyl sulfoxide (DMSO) group ($3.81 \pm 0.25 \times 10^{-5}$ cm/s). This indicates that the soluble form of RES

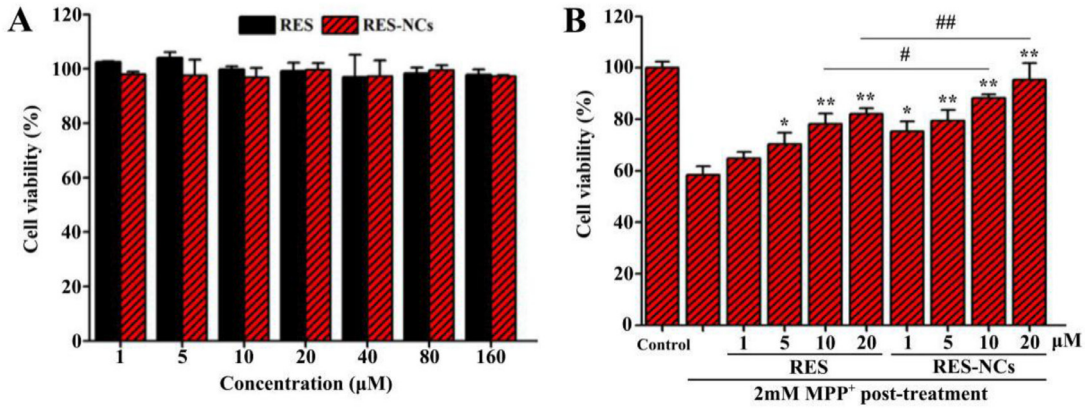

Fig. 3 – RES-NCs protected against MPP^+-mediated cell death. (A) Cell viability after treatment with different concentrations of RES and RES-NCs. The data are presented as means ± SD ($n = 3$). (B) Comparison of cytotoxic effects between RES group and RES-NCs group. The data are presented as means ± SD ($n = 4$). Relative to MPP^+ group: $^*P < 0.05$ and $^{**}P < 0.01$. Relative to RES group: $^{\#}P < 0.05$ and $^{\#\#}P < 0.01$.

exhibits good permeability, and its permeation is not greatly enhanced by RES-NCs. According to our previous report, nanocrystals can be internalized by MDCK cells, followed by their intracellular release, with most being transported in a soluble form across cell monolayers [25]. RES-NCs of a similar size to those in previous report are known to be taken into cells primarily through clathrin-mediated endocytosis [26].

3.4. *RES-NCs protected against MPP^+-mediated cell death*

In vitro toxicity of RES-NCs was assessed in SH-SY5Y cells at different concentrations (1–160 μM) by using MTT analysis. The results demonstrated that RES-NCs exert no obvious cytotoxicity within the indicated concentration range (Fig. 3A). Besides, 58% of cell death was found in 2 mM MPP^+-treated SH-SY5Y cells. Pretreatment with 1, 5, 10 and 20 μM of RES-NCs significantly increased the viability of MPP^+-treated SH-SY5Y cells (75%, 79%, 88% and 95%, respectively) compared to RES group.

3.5. *In vivo toxicity evaluation*

The *in vivo* toxicity analysis of RES-NCs was carried out according to the OECD Guidelines of the Testing of Chemicals [27]. Due to the whole-body transparency of zebrafish, its phenotypical and morphological changes could be visually observed throughout the experiment. Given its high structural and functional similarity of biological barriers to human [28], zebrafish was used to evaluate the *in vivo* toxicity of RES-NCs. In particular, the *in vivo* toxic effects of different concentrations (25, 50, 100 and 150 μg/ml) of RES-NCs were investigated on zebrafish embryos at 6 hpf (Fig. 4A). We were able to observe these embryos for any changes in blood flow, developmental delays, or other malformations at 24, 48, 72, and 96 hpf. We did not detect any evidence of morphological changes in zebrafish embryo or larval zebrafish following RES-NCs treatment (Fig. 4B). It was found that there were no significant differences in the survival and hatching rates at 72 hpf between RES-NCs treatment and control groups (Fig. 4C and Fig. 4D). These results indicate that RES-NCs exert no toxic effect on zebrafish, consistent with our findings of *in vitro* cytotoxicity study.

3.6. *RES-NCs pharmacokinetics*

To investigate whether RES-NCs could enhance the bioavailability and brain uptake of RES, *in vivo* pharmacokinetic analysis was performed in the brain and plasma of SD rats administered with 4 mg/kg of RES or RES-NCs. As shown in Fig. 5A and Table 2, a peak plasma concentration of 2.97 ± 0.46 μg/ml was detected at 2.11 h, indicating that RES-NCs tended to be absorbed rapidly. RES-NCs were thereafter quickly eliminated from serum, with a $T_{1/2}$ of 1.45 h. Relative to control group, the values of C_{max} and AUC_{0-t} in RES-NCs group were enhanced by 3.09- and 3.52-fold, respectively. The AUC_{0-t} of RES obtained from RES-NCs administration was comparatively higher than that reported by Hao et al. [29]. However, it is noticeable that the plasma MRT_{0-t} of rats treated with RES-NCs was relatively similar to that of non-treated rats. The increased oral bioavailability of RES-NCs is possibly due to their small particle size and large surface area [30], as supported by the *in vitro* dissolution testing.

In brain pharmacokinetic study, the values of C_{max} and AUC_{0-t} were significantly higher in RES-NCs group (0.26 ± 0.02 μg/g and 2.61 ± 0.21 μg·h/g, respectively) in comparison with control group (0.11 ± 0.01 μg/g and 1.12 ± 0.18 μg·h/g, respectively) (Fig. 5B and Table 2). The accumulation of RES in the brain tissues following an oral administration of RES-NCs can be explained by the absorption of RES into the circulatory system and subsequently enters the brain across the blood-brain barrier (BBB) [25]. In addition, the stabilizer HPMC in RES-NCs serves as a brain penetration enhancer, which makes the higher amount of drug in the brain tissues. Moreover, the $T_{1/2}$ (3.32 ± 0.14 h) of RES-NCs was delayed in the brain compared to that in the plasma (1.45 ± 0.16 h), suggesting that the elimination of RES from the brain is much slower than the

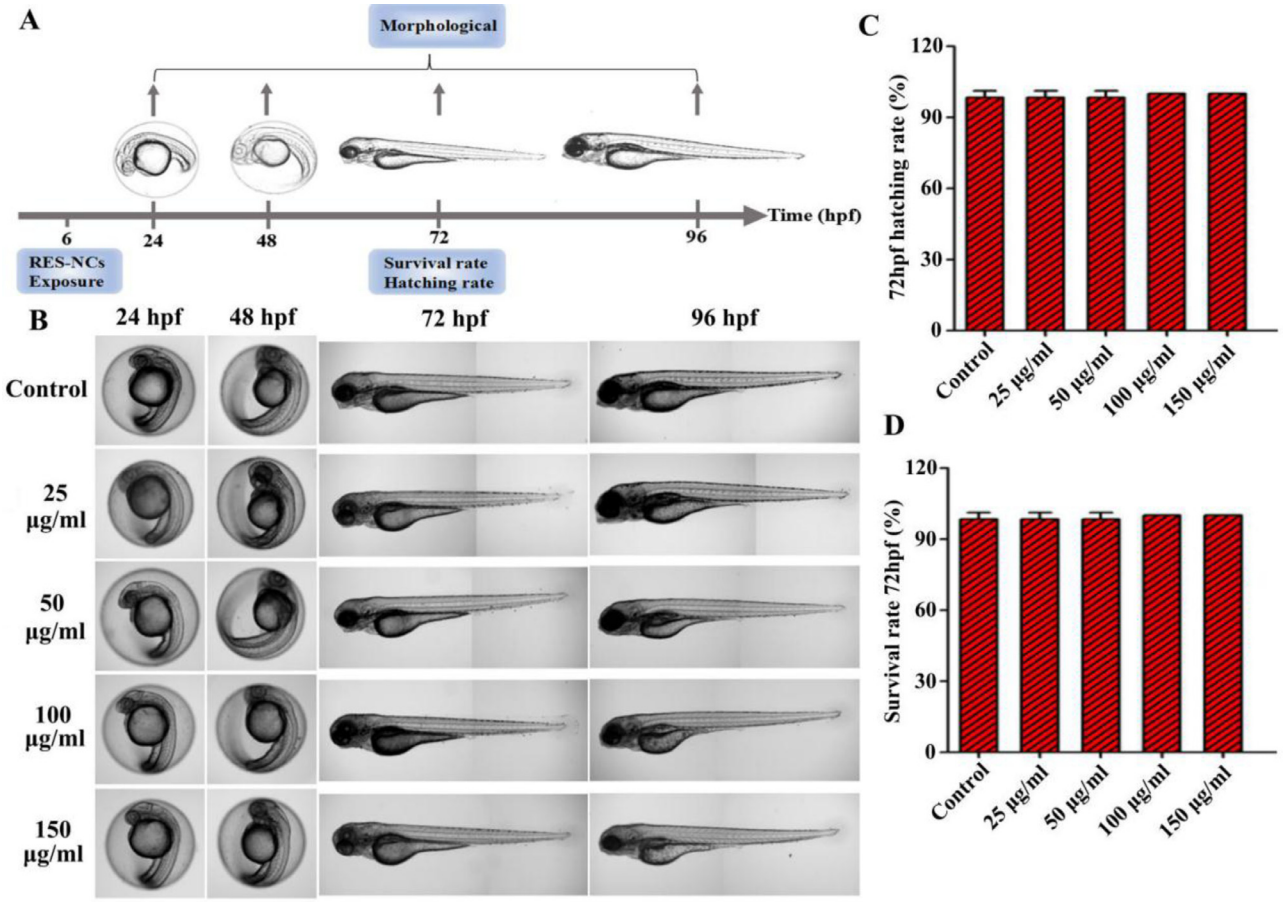

Fig. 4 – *In vivo* toxicity evaluation of RES-NCs. (A) Experimental design of zebrafish toxicity analysis. (B) The morphological changes in zebrafish embryos at 24–96 hpf in RES-NCs treated samples. Scale bar: 250 μm. The hatching (C) and survival (D) rates of zebrafish larvae exposed to different concentrations of RES-NCs.

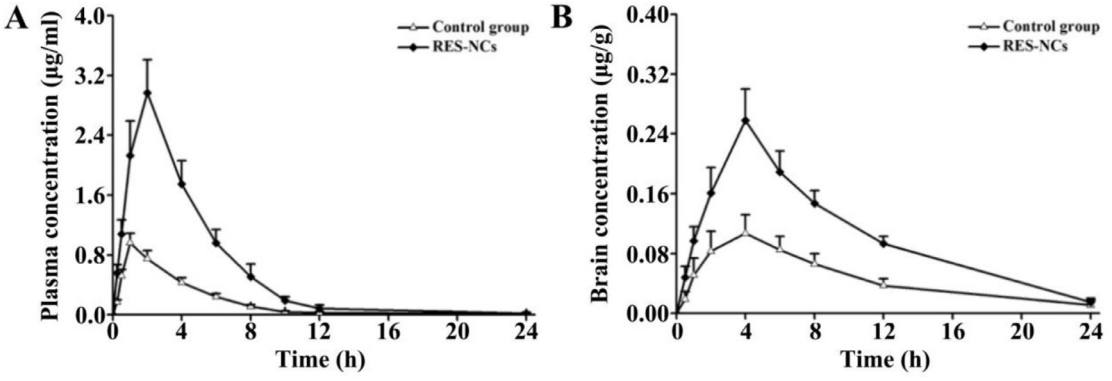

Fig. 5 – Pharmacokinetic profiles for RES-NCs-treated rats. (A) Plasma concentrations over time (means ± SD, $n = 6$). (B) Brain concentrations over time (means ± SD, $n = 3$).

blood. Collectively, RES-NCs formulation may offer a means of improving RES absorption and brain accumulation *in vivo*. However, the *in vivo* fate of RES-NCs after oral administration warrants further investigation.

3.7. *RES-NCs improved MPTP-mediated locomotor deficiencies*

The experimental design of pharmacodynamic study is illustrated in Fig. 6A. MPTP-induced acute mice displayed

Table 2 – RES-NCs pharmacokinetics ($n = 6$ in the plasma, and $n = 3$ in the brain).

Parameters	Plasma		Brain	
	Control group	RES-NCs	Control group	RES-NCs
$T_{1/2}$ (h)	2.28 ± 0.35	1.45 ± 0.16**	2.50 ± 0.21	3.32 ± 0.14**
T_{max} (h)	1.04 ± 0.02	2.11 ± 0.05*	4.27 ± 0.06	4.09 ± 0.03
C_{max} (μg/ml)	0.96 ± 0.21	2.97 ± 0.46**	0.11 ± 0.01	0.26 ± 0.02**
$AUC_{0\text{-}t}$ (μg·h/ml)	4.01 ± 0.68	14.13 ± 1.57**	1.12 ± 0.18	2.61 ± 0.21**
$MRT_{0\text{-}t}$ (h)	4.14 ± 0.74	4.13 ± 0.42	7.96 ± 0.62	7.78 ± 0.38
F	100%	352%	–	–

* $P < 0.05$ and ** $P < 0.01$ *vs* control.

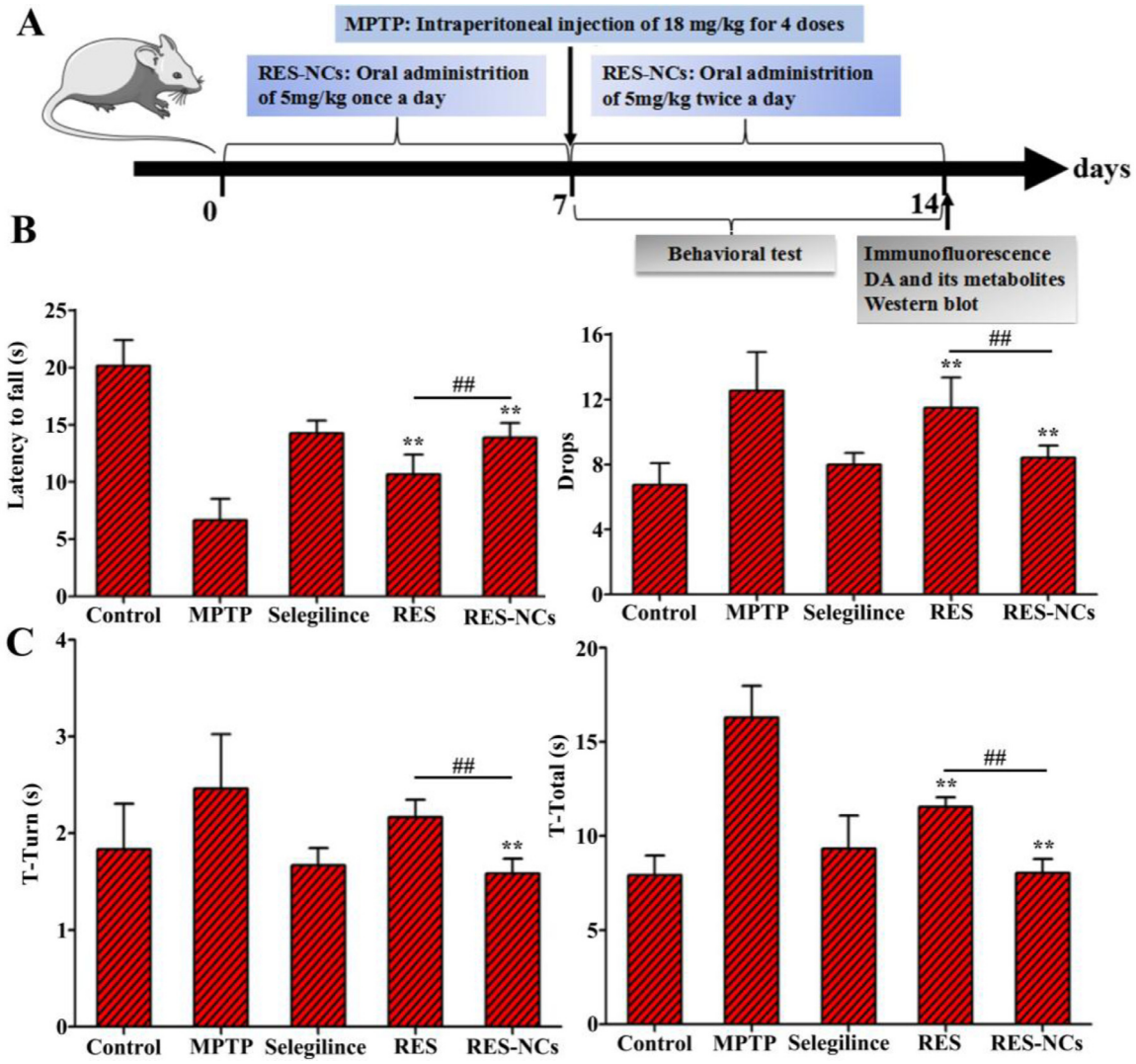

Fig. 6 – Effects of RES-NCs on the behavioral deficits of PD mice induced by MPTP injection. (A) Experimental design of pharmacodynamic study. Rotarod (B) and pole tests (C) were performed 7 days following injecting MPTP. Data are means ± SD ($n = 8$). Relative to MPTP group: *$P < 0.05$ and **$P < 0.01$. Relative to RES group: #$P < 0.05$ and ##$P < 0.01$.

clinical characteristics of PD, such as loss of motor function related to TH^+ neuron depletion and low DA levels in the brain [31]. To examine the impact of RES-NCs on the balance and coordination performance of MPTP-lesioned mice, their locomotor activities (e.g. the latency to fall and the number of drops) were tested by a rotarod assay. Notably, RES-NCs treatment increased the time of latency to fall and reduced the number of drops (Fig. 6B). In addition, pole test was conducted to investigate the influence of RES-NCs on bradykinesia in MPTP-lesioned mice. The results demonstrated that

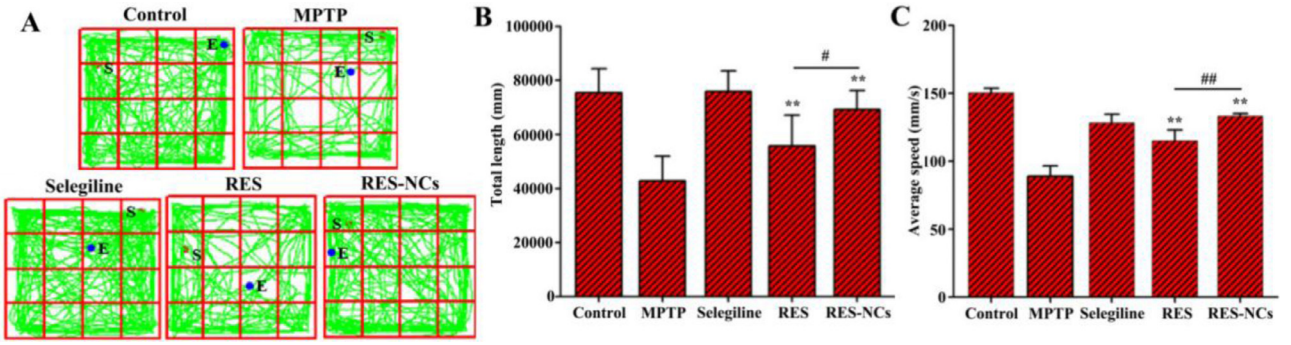

Fig. 7 – Open-field test results. (A) Representative mouse movement (in green) in an open-field box. Total distance travelled (B) and average speed of travel (C) for the differently treated mice. Results are means ± SD ($n = 8$). Relative to MPTP group: *$P < 0.05$ and **$P < 0.01$. Relative to RES group: $^{\#}P < 0.05$ and $^{\#\#}P < 0.01$.

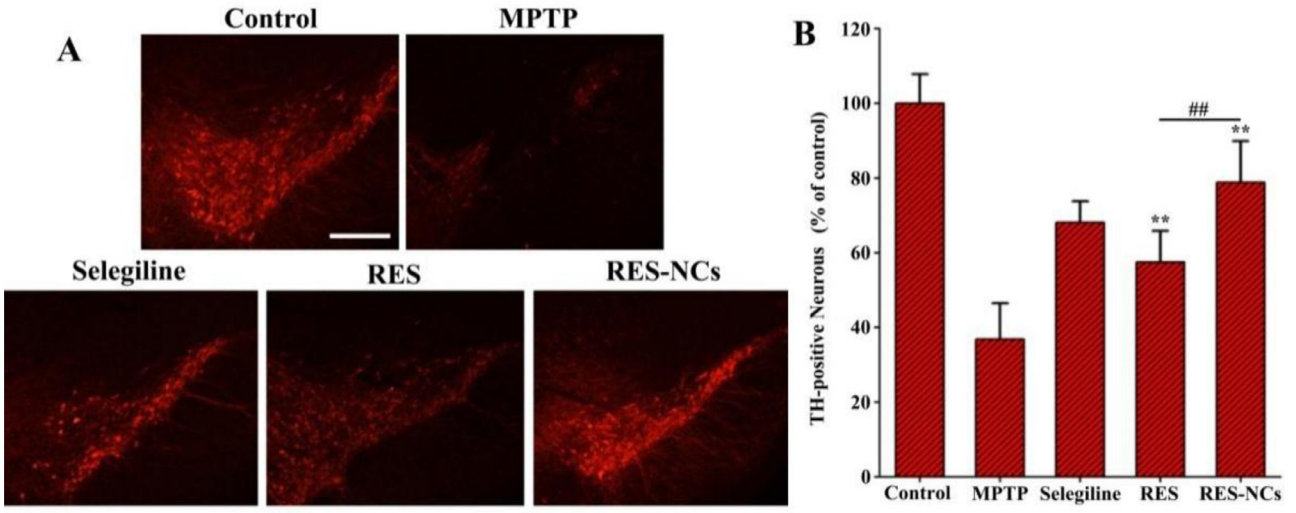

Fig. 8 – RES-NCs shielded against TH^+ neuron lose in the substantia nigra of MPTP-treated mice. (A) Representative images of TH-immunostained brain sections from mice treated as indicated. Scale bar: 250 μm. (B) Quantification of numbers of TH^+ neurons. Results are means ± SD ($n = 5$). Relative to MPTP group: **$P < 0.01$. Relative to RES group: $^{\#\#}P < 0.01$.

RES-NCs significantly decreased the turnaround time (t-turn) and total time to reach the bottom (t-total) 7 days following MPTP injection (Fig. 6C). As shown in Fig. 7, the exploratory behaviors and spontaneous motor activity were evaluated using an open-field test. The spontaneous motor activity maps revealed that MPTP-lesioned mice exhibited an apparent decrease in their moving distance (Fig. 7A). RES-NCs treatment, however, significantly increased total movement distance and average travelled speed of PD mice (Fig. 7B and C). These findings suggest that RES-NCs can reverse the balance and coordination deficits of MPTP-lesioned mice.

3.8. *RES-NCs prevented neurotoxicity induced by MPTP*

The amount of TH^+ neurons in the substantia nigra pars compacta represents a severity index of dopaminergic neuronal damage in MPTP-induced PD mouse model [32]. When imaging the brain tissues of MPTP-treated mice, we observed clear evidence of the neuroprotective abilities of RES-NCs *in vivo* (Fig. 8A). In total, RES-NCs-treated PD mice increased 42% of dopaminergic neurons compared to non-treated PD mice (Fig. 8B). The level of TH^+ neurons was markedly higher in RES-NCs group than in RES group (Fig. 8B). Treatment with MPTP was also associated with reduced striatal DA, 3,4-dihydroxyphenylacetic acid (DOPAC), and homovanillic acid (HVA) levels. Importantly, treatment with RES-NCs reversed the low metabolite and dopamine levels in MPTP-treated PD model mice (Table 3).

3.9. *RES-NCs mediated neuroprotection in PD model mice via activating in Akt/Gsk3β signaling pathway*

To elucidate the molecular mechanisms underlying the protective effects of RES-NCs, both Akt and Gsk3β signaling pathways were investigated in MPTP-lesioned mice. Western blotting was applied to measure the protein levels of Akt and Gsk3β as well as the levels of phosphorylated Akt (p-Akt) and phosphorylated Gsk3β (p-Gsk3β). The results demonstrated that the decreased levels of p-Akt and p-Gsk3β in MPTP-lesioned mice were significantly induced

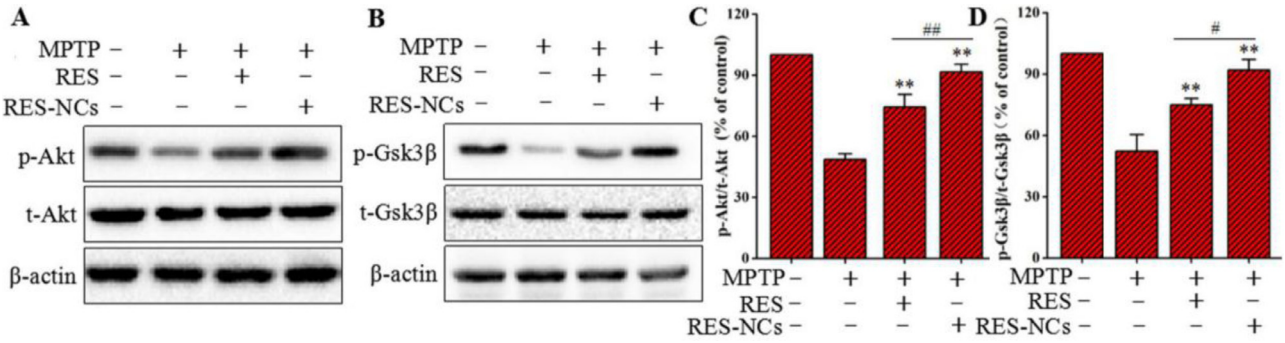

Fig. 9 – Expression levels of Akt and Gsk3β in PD mice treated with RES or RES-NCs. (A) p-Akt/t-Akt, and (B) p-Gsk3β/t-Gsk3β were measured via Western blotting. Protein levels for p-Akt/t-Akt (C) and p-Gsk3β/t-Gsk3β (D) were quantified via densitometry. β-actin was used to normalize protein expression. Relative to MPTP group: $^{**}P < 0.01$. Relative to RES group: $^{\#}P < 0.05$ and $^{\#\#}P < 0.01$.

Table 3 – Metabolite levels in treated mice (μg/g tissue, $n = 4$).

Group	DA	DOPAC	HVA
Control	13.16 ± 2.75	1.52 ± 0.33	4.74 ± 0.81
MPTP	3.59 ± 0.48**	0.77 ± 0.20**	3.25 ± 0.57**
Selegiline	11.23 ± 3.26*##	1.38 ± 0.25*##	4.03 ± 0.76*#
RES	7.81 ± 1.53**##	0.81 ± 0.21**#	2.75 ± 0.49*##
RES-NCs	9.92 ± 2.74**##▲▲	1.09 ± 0.13**##▲	3.53 ± 0.66*#▲▲

Relative to control: $^{*}P < 0.05$ and $^{**}P < 0.01$. Relative to MPTP group: $^{\#}P < 0.05$ and $^{\#\#}P < 0.01$. Relative to RES group: $^{▲}P < 0.05$ and $^{▲▲}P < 0.01$.

by RES-NCs, and their levels were remarkably higher in RES-NCs group compared to the unformulated RES group (Fig. 9A and B). Furthermore, the densitometric values of p-Akt/t-Akt (total Akt) and p-Gsk3β/t-Gsk3β (total Gsk3β) were calculated to further verify the roles of RES-NCs on these signaling pathways. The percentage values of p-Akt/t-Akt and p-Gsk3β/t-Gsk3β were markedly greater in RES-NCs group compared to MPTP and RES groups (Fig. 9C and D). These results indicate the essential role of Akt/Gsk3β signaling pathway during the neuroprotection of RES-NCs against PD.

4. Conclusions

In summary, RES-NCs with HPMC stabilizer were successfully developed using antisolvent precipitation approach. RES-NCs significantly enhanced the *in vitro* dissolution rate of RES, and improved its oral absorption and brain accumulation. Moreover, RES-NCs treatment improved behavioural deficits, attenuated the loss of dopaminergic neurons, and enhanced levels of DA and its associated metabolites in PD mice. The molecular mechanisms underlying the neuroprotective effect of RES-NCs might be at least partially attributed to Akt/Gsk3β signaling pathway. Taken altogether, these results clearly demonstrate that RES-NCs are an effective strategy to improve RES bioavailability, making them a promising potential therapeutic approach to treat PD.

Conflict of interest

The authors declare that they have no competing interests.

Acknowledgement

This study was supported by the Guangdong Provincial Natural Science Foundation of China (2018A030310623), Research Fund of University of Macau (MYRG2018-00207-ICMS and SRG2017-00095-ICMS), National Natural Science Foundation of China (81673627), and Guangzhou Science Technology and Innovation Commission Technology Research Projects (201805010005).

Supplementary materials

Supplementary material associated with this article can be found, in the online version, at doi:10.1016/j.ajps.2019.04.003.

REFERENCES

[1] Maurya H, Kumar S. Current medication trends and global impact on neurodegenerative disorders. J Pharm Pharmacol 2018;6(1):9.
[2] Yu M, Suo H, Liu M, Cai L, Liu J, Huang Y, et al. NRSF/REST neuronal deficient mice are more vulnerable to the neurotoxin MPTP. Neurobiol Aging 2013;34(3):916–27.
[3] Jamebozorgi K, Taghizadeh E, Rostami D, Pormasoumi H, Barreto GE, Hayat SMG, et al. Cellular and molecular aspects of Parkinson treatment: future therapeutic perspectives. Mol Neurobiol 2018;5:1–13.
[4] Abbott NJ, Patabendige AA, Dolman DE, Yusof SR, Begley DJ. Structure and function of the blood-brain barrier. Neurobiol Dis 2010;37(1):13–25.
[5] Chen Y, Liu L. Modern methods for delivery of drugs across the blood-brain barrier. Adv Drug Deliv Rev 2012;64(7):640–65.
[6] Srivastav S, Fatima M, Mondal AC. Important medicinal herbs in Parkinson's disease pharmacotherapy. Biomed Pharmacother 2017;92:856–63.
[7] Song JX, Sze SC, Ng TB, Lee CK, Leung GP, Shaw PC,

et al. Anti-Parkinsonian drug discovery from herbal medicines: what have we got from neurotoxic models? J Ethnopharmacol 2012;139(3):698–711.
[8] Bastianetto S, Menard C, Quirion R. Neuroprotective action of resveratrol. Biochim Biophys Acta 2015;1852(6):1195–201.
[9] Abolaji AO, Adedara AO, Adie MA, Vicente-Crespo M, Farombi EO. Resveratrol prolongs lifespan and improves 1-methyl-4-phenyl-1,2,3,6-tetrahydropyridine-induced oxidative damage and behavioural deficits in Drosophila melanogaster. Biochem Biophys Res Commun 2018;503(2):1042–8.
[10] Khan MM, Ahmad A, Ishrat T, Khan MB, Hoda MN, Khuwaja G, et al. Resveratrol attenuates 6-hydroxydopamine-induced oxidative damage and dopamine depletion in rat model of Parkinson's disease. Brain Res 2010;1328:139–51.
[11] Zeng W, Zhang W, Lu F, Gao L, Gao G. Resveratrol attenuates MPP(+)-induced mitochondrial dysfunction and cell apoptosis via AKT/GSK-3beta pathway in SN4741 cells. Neurosci Lett 2017;637:50–6.
[12] Li B, Wegiel LA, Taylor LS, Edgar KJ. Stability and solution concentration enhancement of resveratrol by solid dispersion in cellulose derivative matrices. Cellulose 2013;20(3):1249–60.
[13] Suktham K, Koobkokkruad T, Wutikhun T, Surassmo S. Efficiency of resveratrol-loaded sericin nanoparticles: promising bionanocarriers for drug delivery. Int J Pharm 2018;537(1–2):48–56.
[14] Ramalingam P, Ko YT. Improved oral delivery of resveratrol from N-trimethyl chitosan-g-palmitic acid surface-modified solid lipid nanoparticles. Colloids Surf B Biointerfaces 2016;139:52–61.
[15] Summerlin N, Qu Z, Pujara N, Sheng Y, Jambhrunkar S, McGuckin M, et al. Colloidal mesoporous silica nanoparticles enhance the biological activity of resveratrol. Colloids Surf B Biointerfaces 2016;144:1–7.
[16] Siu FY, Ye S, Lin H, Li S. Galactosylated PLGA nanoparticles for the oral delivery of resveratrol: enhanced bioavailability and *in vitro* anti-inflammatory activity. Int J Nanomed 2018;13:4133–44.
[17] Fontana F, Figueiredo P, Zhang P, Hirvonen JT, Liu D, Santos HA. Production of pure drug nanocrystals and nano co-crystals by confinement methods. Adv Drug Deliv Rev 2018;131:3–21.
[18] Pawar VK, Singh Y, Meher JG, Gupta S, Chourasia MK. Engineered nanocrystal technology: *in vivo* fate, targeting and applications in drug delivery. J Control Release 2014;183:51–66.
[19] Xia D, Gan Y, Cui F. Application of precipitation methods for the production of water-insoluble drug nanocrystals: production techniques and stability of nanocrystals. Curr Pharm Des 2014;20(3):408–35.
[20] Lu Y, Qi J, Dong X, Zhao W, Wu W. The *in vivo* fate of nanocrystals. Drug Discov Today 2017;22(4):744–50.
[21] Moschwitzer JP. Drug nanocrystals in the commercial pharmaceutical development process. Int J Pharm 2013;453(1):142–56.
[22] Chen C, Wang L, Cao F, Miao X, Chen T, Chang Q, et al. Formulation of 20(S)-protopanaxadiol nanocrystals to improve oral bioavailability and brain delivery. Int J Pharm 2016;497(1–2):239–47.
[23] Chen T, Li C, Li Y, Yi X, Wang R, Lee SM, et al. Small-sized mPEG-PLGA nanoparticles of schisantherin A with sustained release for enhanced brain uptake and anti-Parkinsonian activity. ACS Appl Mater Interfaces 2017;9(11):9516–27.
[24] Zhou H, Wang C, Deng T, Tao R, Li W. Novel urushiol derivatives as HDAC8 inhibitors: rational design, virtual screening, molecular docking and molecular dynamics studies. J Biomol Struct Dyn 2018;36(8):1966–78.
[25] Chen T, Li C, Li Y, Yi X, Lee SM, Zheng Y. Oral delivery of a nanocrystal formulation of Schisantherin A with Improved Bioavailability and Brain Delivery for the Treatment of Parkinson's Disease. Mol Pharm 2016;13(11):3864–75.
[26] Rejman J, Oberle V, Zuhorn IS, Hoekstra D. Size-dependent internalization of particles via the pathways of clathrin- and caveolae-mediated endocytosis. Biochem J 2004;377(1):159–69.
[27] Sobanska M, Scholz S, Nyman AM, Cesnaitis R, Gutierrez Alonso S, Kluver N, et al. Applicability of the fish embryo acute toxicity (FET) test (OECD 236) in the regulatory context of registration, evaluation, authorisation, and restriction of chemicals (REACH). Environ Toxicol Chem 2018;37(3):657–70.
[28] Fleming A, Diekmann H, Goldsmith P. Functional characterisation of the maturation of the blood-brain barrier in larval zebrafish. PLoS One 2013;8(10):e77548.
[29] Hao J, Gao Y, Zhao J, Zhang J, Li Q, Zhao Z, et al. Preparation and optimization of resveratrol nanosuspensions by antisolvent precipitation using Box-Behnken design. AAPS PharmSciTech 2015;16(1):118–28.
[30] Ndlovu ST, Ullah N, Khan S, Ramharack P, Soliman M, de Matas M, et al. Domperidone nanocrystals with boosted oral bioavailability: fabrication, evaluation and molecular insight into the polymer-domperidone nanocrystal interaction. Drug Deliv Transl Res 2018;9(1):284–97.
[31] Seo J, Lee Y, Kim BS, Park J, Yang S, Yoon HJ, et al. A non-human primate model for stable chronic Parkinson's disease induced by MPTP administration based on individual behavioral quantification. J Neurosci Methods 2018;311:277–87.
[32] Liu L, Peritore C, Ginsberg J, Shih J, Arun S, Donmez G. Protective role of SIRT5 against motor deficit and dopaminergic degeneration in MPTP-induced mice model of Parkinson's disease. Behav Brain Res 2015;281:215–21.